JOURNAL OF HIGH-FREQUENCY COMMUNICATION TECHNOLOGIES
Vol. 01 (01) (2023), pp.12-23

Optimum Design of a Novel Electronically Reconfigurable Reflectarray Antenna for X/Ku Band Applications

Vidhyashree Suresh[1*]

[1] Department of ECE, Sri Sivasubramaniya Nadar College of Engineering, Kalavakkam, Chennai, 603110, India, *E-mail address:* vidhyashrees@ssn.edu.in

Abstract

The frequency reconfigurable reflectarray (RRA) reported in this paper provides a pencil beam at three frequencies, captivating the need for satellite broadcast television at uplink and downlink frequencies in the Ku and X-bands. The unit cell structure with a periodicity of $0.49\lambda_0$ comprises three concentric square rings with variations of two inner concentric rings contributing to uplink frequency. Two delay lines connected with Positive-Intrinsic-Negative (PIN) diodes are varied to compensate for phase variation at downlink and X-band frequencies. To achieve such frequency reconfiguration, a unit cell is simulated based on an infinite array approach and in integration with four PIN diodes to produce a reflection phase variation of 525°, 415°, and 308° at 14.34 GHz for uplink operation, 12.2 GHz for downlink, and 11.9 GHz for X-band performance, respectively. By switching PIN Diodes in ON and OFF state conditions, frequency reconfiguration within bands is achieved. With a periodicity of $0.49\lambda_0$ (10.5 mm), a 15 × 15 array with 225 elements is constructed using the designed unit cell in square planar geometry. The paper reports a simulated maximum gain of 25.77 dBi, 25.13 dBi, and 22.7 dBi and 40.22%, 26.46%, and 25.36% of aperture efficiency at 14.34 GHz, 12.2 GHz, and 11.9 GHz, respectively. A –3 dB gain bandwidth of 8.37%, 4.92%, and 12.18% is achieved at the three operating frequencies by simulation. Hence this RRA serves as an emulous alternative to parabolic reflectors and phased array antennas in deep space communication and direct broadcast satellite applications satisfying the high gain pencil beam requirements.

Keywords: *X/Ku band; Frequency reconfiguration; PIN diodes; Reflectarray;True-time delay line*

1. Introduction

Microstrip reconfigurable reflectarrays (RRA) (Pozar, 2003) have emerged as a revolutionary breakthrough in printed antenna technology, providing multi-beam synthesis for distinct applications like military applications, high-resolution imaging radars, remote sensing, weather monitoring, backhauls, maritime vessel traffic control, defense tracking, air traffic, etc. By inheriting salient features of both reflectors and printed phased arrays, the planar reflecting surface offers an added advantage in terms of shape and compactness compared to parabolic reflectors. Reflectarray Antenna (RA) has prominent features like a low-profile structure, simple spatial feed,

[*]**Corresponding author**
Received: 17^{th}, November 2022, Revised: 15^{th} January, 2023 Accepted: 26^{th} January 2023 and available online 11^{th} February 2023
https://doi.org/10.58399/DAUK9418

This work is licensed under a Creative Commons Attribution 4.0 License(CC BY 4.0).
For more information, see https://creativecommons.org/licenses/by/4.0/

high gain with pencil beam width, reconfigurability, flexible installation, and low production cost (Arslan and Alamgir, 2017), but it suffers from the shortcoming of narrow bandwidth. Bandwidth improvement has been attempted using attractive approaches, including a cross-dipole of variable size (Chen et al., 2013), concentric rings (Barriuso et al., 2011), circular split rings with two-phase delay lines (Malfajani and Atlasbaf, 2014), and multi-layer stacking of elements (Encinar and Zornoza, 2004). Reconfiguration in reflectarray is required for sharing the same aperture in different bands by integrating with active elements. Reconfiguration in RA is achieved by modifying its properties, such as frequency, radiation, and polarization, in a dynamic and controlled manner using electrical and mechanical actuators or tunable materials. In the early phases of reconfiguration, a 5×1 RRA consisting of a rotating circular disk is developed for beam scanning by rotating the elements clockwise and counter-clockwise using mechanical actuators (Fusco, 2005).

Such actuators have the major drawbacks of increased motor size and cost. As a cost-effective solution, varactors, being one of the electronically tunable elements, are utilized in multilayer, 3×15 aperture-coupled RRA (Venneri et al., 2012) & (Venneri et al., 2013). The papers report an effective mechanism to realize dual-frequency operation, achieving a full phase tuning range with a single varactor diode. The antenna employed suffers from limitations like increased thickness and an increase in sensitivity due to a coupling effect resulting in a reduction in bandwidth. To overcome these limitations, several single-layer, single-band, and dual-band RRAs are presented in (Hum et al., 2005), (Tayebi et al., 2015), (Abdelrahman et al., 2017) & (Liu et al., 2018). In (Abdelrahman et al., 2017), the 330° phase variation is obtained by a proper inclusion of capacitive and inductive loads in the form of a varactor-loaded line and stub.

Beam scanning up to 45° is achieved at an operating frequency of 10 GHz. Similarly, researchers in (Liu et al., 2018) have obtained continuous beam scanning within ±45° using 81 element arrays developed with unit cells having two varactors between horizontal slots of each element. The proposed unit cell offers a 375° phase range and 3.09% bandwidth. Although varactors have many merits, like medium cost, negligible power consumption, nanosecond speed, less mounting complexity, and continuously switching the beam, a small fluctuation in direct current (dc) biasing may lead to large beam deterioration. Hence, researchers in (Guclu et al., 2012), (Bayraktar et al., 2012), (Perruisseau-Carrier and Skrivervik, 2008) & (Wu et al., 2008) have utilized another category of electronically tunable elements, microelectro mechanical systems (MEMS), to obtain full 360° phase variation. In (Guclu et al., 2012), researchers have developed a RA using split rings integrated into radio frequency (RF) MEMS switches to achieve beam switching to ±35° and ±24° at 24.4 GHz and 35.5 GHz.

Proper biasing of the MEMS switches produces angular rotation of the split rings, which in turn controls the 360° phase variation. A similar result is obtained using aperture-coupled elements in (Bayraktar et al., 2012). Digitally controlled MEMS switches reported in (Perruisseau-Carrier and Skrivervik, 2008) & (Wu et al., 2008) overcome the problem of voltage imprecision faced in analog types, which causes a reduction in sensitivity. MEMS devices have advantages like very low loss and negligible power consumption, but their complex design and high cost become serious hindrances to their usage. In RRAs implemented using tunable materials (Hu et al., 2008), (Perez-Palomino et al., 2013) & (Perez-Palomino et al., 2015) like graphene and liquid crystals, the requirement of a biasing circuit on the substrate layer is minimized. The RAs reported in (Perez-Palomino et al., 2015) operate between 96 GHz and 104 GHz frequencies producing beam steered over 55° angular range.

But, in all RAs developed using liquid crystals, the integration of crystal materials in the RA panel is a challenging task. Thus, to overcome these challenges, PIN diodes are selected as a tradeoff in terms of cost, a less sensitive biasing circuit, and design complexity in multi-layer RRA structures (Kamoda et al., 2011), (Carrasco et al., 2012) & (Luyen et al., 2019). In (Kamoda et al., 2011), 160×160 reflecting elements operating at 60 GHz with a single-bit digital phase shifter and a PIN diode are designed for the beam-forming application. These multilayer RRAs suffer the sensitivity effect due to coupling and need to be fabricated carefully for perfect alignment between radiating layers. To avoid these limitations, single-layer RRAs are described in (Han et al., 2019), (Li and Abbosh, 2015), (Yang et al., 2017) & (Han et al., 2004). A wideband 1-bit 12×12 reconfigurable beam-scanning RA is designed at 5 GHz (Han et al., 2019) producing beam steering

to 22° with a peak measured gain of 14.1 dBi.

The proposed unit cell offers a 350° phase shift by varying the length of the circular stub using a PIN diode. The phase variation of the RA gets limited due to the reduction in the reactance of the RF choke used in the PIN diode biasing circuit. From the literature survey, it is evident that dual-band or frequency reconfiguration within two frequencies is attempted, while reconfiguration for three frequencies needs to be addressed.

In the proposed design, a simulated gain of 25.55 dB for uplink, 24.86 dB for downlink, and 22.65 dB for the X band are reported. Similarly, 3 dB gain bandwidths of 8.37%, 4.92%, and 12.18% are obtained at respective frequencies. These 3 dB gain bandwidth values obtained using 225 elements are higher compared to other papers reported in the literature. Due to its novel RA structure and better radiation performance, this antenna is well-suited for satellite broadcast television at uplink and downlink frequencies. Based on the study made through the literature survey, a 15×15 RRA

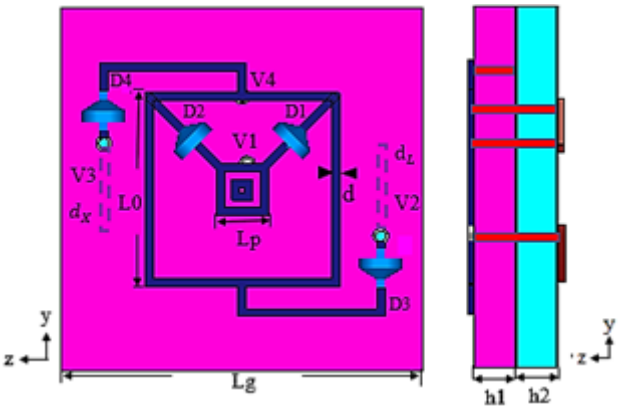

Figure 1. Proposed RRA element (a) Front view (b) Side view

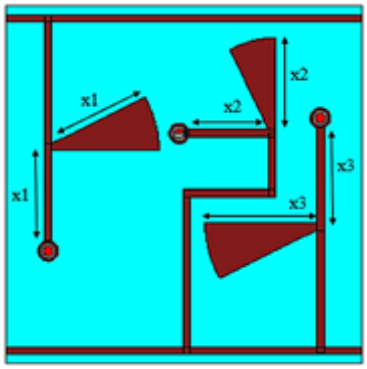

Figure 2. Modified Defected Ground Structure

structure is constructed with 225 elements to obtain frequency reconfiguration controlled using four PIN diodes. The proposed structure operates at uplink and downlink frequencies of 14.34 GHz and 12.2 GHz, respectively, and an X-band frequency of 11.9 GHz. In the OFF condition of all PIN diodes, the proposed unit cell produces a 525° phase variation at the uplink frequency. The phase range of 415° is obtained at downlink frequency with one PIN diode in ON condition and 308° phase variation at 11.9 GHz with all PIN diodes operated in ON condition. This paper is organized as follows: Section 2 discusses the design and analysis of the proposed RA unit cell structure. The implementation of the RA antenna design and its fabrication details are presented in Section 3. Section 4 explains the simulation results of the proposed RA structure. The design and performance characteristics of the array are also summarized in this section. The performance comparison of the RRA proposed in this work discussed in the survey is also tabulated in this section.

2. Unit Cell Design and Analysis

In this paper, a $10.5 \times 10.5mm$ ($0.49\ \lambda_0$) unit cell is developed on a $h_1 = 1.575$ mm thick Taconic TLY-5 substrate with relative permittivity, $\varepsilon_r = 2.2$ and 0.0009 loss tangent value backed by a ground layer of thickness 0.035 mm. For providing additional support to the ground, this structure is held up by an Fr4 substrate $\varepsilon_r = 4.4$ mm of thickness, $h_2 = 1.6$ mm with a biasing circuit present on the bottom surface. For designing square ring structures, the permittivity of two substrates is mentioned as ε_{r1}, ε_{r2} and height as h_1 and h_2. Initially, the total thickness (h_t) and effective permittivity (ε_{eq}) values need to be calculated using Equ's. 1 & 2 (Murugesan et al., 2021) as

$$h_t = h_1 + h_2 \tag{1}$$

$$\varepsilon_{reff} = \frac{\varepsilon_{r1}h_1 + \varepsilon_{r2}h_2}{h_1 + h_2} \tag{2}$$

The proposed unit cell structure of the frequency RRA is depicted in Fig. 1. The element comprises three concentric square rings where the inner and middle square loop dimensions are varied to obtain different phase ranges over the required band of operation. The inner two rings are separated by a uniform gap, while the outer ring gap is increased to enclose the PIN diodes. The size of the innermost concentric ring, L_i, is varied concerning the middle ring as $L_i = L_p - 2d$. Two delay lines are integrated on the opposite faces of the outermost ring, whose lengths are varied to obtain an increased phase range. Detailed dimensions of the proposed element are given in Table 2. The unit cell is designed and developed for uplink frequency, with two PIN diodes (D1 and

Table 1. Equivalent Circuit Parameters of PIN Diode

Parameter	ON State	OFF State
R	5.2 Ω	–
L	30 pH	30 pH
C	–	0.035 pF

Table 2. Design Parameters of RRA Element

Parameter	Description	Value (mm)
L_g	Unit cell size	10.5
L_0	Length of the outer loop	7.5
L_p	Length of the inner loop	5.5
d	Width of the loop	0.3
h	Height of the substrate	1.575

D2) integrated between the outermost ring and middle ring as shown in Fig. 1(a). The diodes are driven by a suitable biasing circuit as shown in Fig. 2. Four vias of diameter 0.6 mm, as shown in Fig. 1(b), are used for connecting the diodes to V_{CC} and ground.

The via on the outermost ring connects the cathodes of all diodes to the ground terminal through a common channel interconnecting all cells in the array. A common via on the middle ring connects the anodes of diodes D1 and D2 to the power supply, whereas vias on the upper and lower delay lines supply diodes D3 and D4. To avoid the appearance of the grating lobes, the periodicity of the proposed element is selected as 10.5 mm, corresponding to 0.49 λ. Regarding the mutual coupling behaviour, the unit cell is modelled to be distributed on an infinite lattice (Floquet modes). Hence, the effect of the incidence of the impinging waves and coupling is assumed to be identical, as shown in Fig. 3. The equivalent circuit parameters of PIN diode are shown in Table 1.

The PIN diode connecting the patch through the biasing circuit to the ground plane alters the resonant property when it is turned ON or OFF according to the dc-biasing voltage. The biasing point is positioned at the minimal electric field point along the non-radiating edges. The biasing circuit, consisting of a quarter-wavelength microstrip acting as an inductive load, is positioned in

the bottom layer. Similarly, a cat ear open-ended radial stub is designed to choke the RF signal. This approach ensures good isolation between dc and RF performance and provides a simplified biasing network. Since the radial stub is positioned on the bottom plane, only two substrate layers are required.

Table 3. Switching Operation of PIN Diodes in the Proposed Structure

Frequency Bands	$f_r(GHz)$	**D1**	**D2**	**D3**	**D4**	**Varying Parameters**	$\angle S_{11}$ **(Degress)**
Uplink	14.34	OFF	OFF	OFF	OFF	L_p	525
Downlink	12.2	OFF	OFF	ON	OFF	d_L	415
X− Band	11.9	ON	ON	ON	ON	d_x	308

The switching operation of PIN Diodes are explained in Table 3. When these two PIN diodes are in the OFF state, the element resonates at the uplink frequency of 14.34 GHz by varying the size of the middle and inner concentric square loops. After optimizing the geometrical parameters, the unit cell is simulated using Computer Simulation Technology (CST) Microwave Studio software based on an infinite array approach with plane wave excitation and unit cell boundary conditions as shown in Fig. 3. The phase response of the unit cell for uplink frequency plotted against varied square loop sizes is depicted in Fig. 4. A linear and smooth reflecting phase curve is achieved with a phase range of 525° at uplink frequency. The surface current distribution on the uplink, downlink, and X-band frequencies is shown in Fig. 5. The high surface current distribution appearing along the middle slot indicates the resonance occurs at 14.34 GHz. Similarly, the downlink and X-band

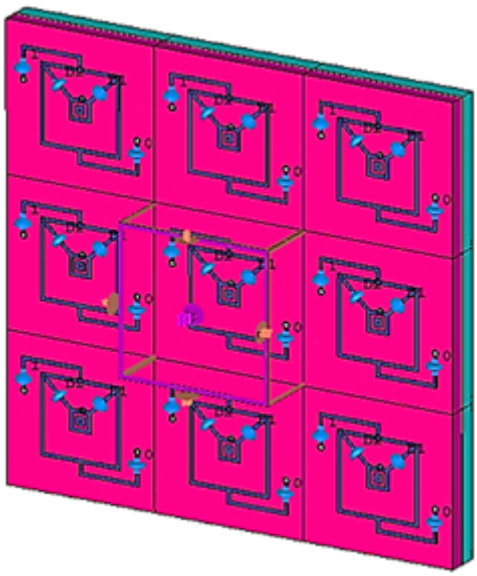

Figure 3. Biasing circuit of proposed unit cell structure, Where x1 = 4.21mm $(\lambda_0/4), x2 = 3.6mm(\lambda_0/4), x3 = 4.39mm(\lambda_0/4)$

resonances occur due to the existence of outer rings. The effect of TE and TM polarization modes over the reflection phase for a normally incident wave at 14.34 GHz is simulated with the proposed unit cell. The variations for TE and TM modes at different incident angles such as 15°, 30°, and 45° in the elevation plane (θ) are depicted in Fig. 5. These variations are observed as a function of the size of the square loop. It is observed that the reflection phase performance for TE mode is stable for all angles of incidence. But for TM mode, the reflection phase deviates at $\theta = 15°$ which could be due to mutual coupling between the elements. As the performance is stable for almost all angles of incidence, the proposed element can be used for developing large offset-fed RAs.

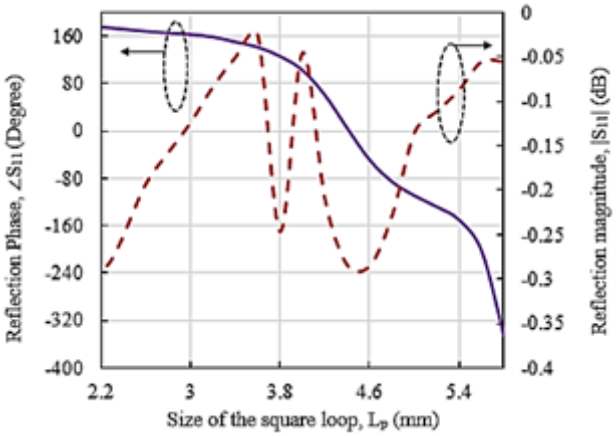

Figure 4. Reflection characteristics of the unit cell at the uplink frequency as a function of L_p

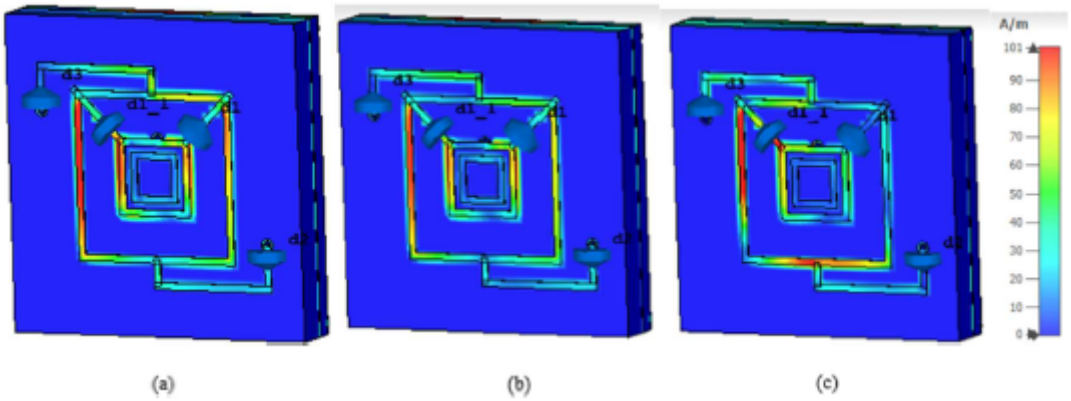

Figure 5. Surface Current distributions (a) 14.34 GHz (b) 12.2 GHz (c) 11.9 GHz

3. Reflectarray Design and Analysis of Reconfigurable Reflectarray

In general, the phase shift required to produce radiation at a distance r_0 in the desired direction (θ_0, φ_0) is determined using the function specified in Eq. 3:

$$\phi_{mn} = k_0(d_i - (x_i \cos\phi_0 + y_i \sin\theta_0) \sin\theta_0 \tag{3}$$

Based on this relationship, the reflection phase required at the uplink frequency is obtained using the MATLAB code. The phase shift to be added to the incident wave by each unit cell for downlink operation is obtained similarly using MATLAB code and compared with the simulated phase shift of the unit cell at uplink frequency. From the difference between these phase shifts, the phase error is calculated as shown in Fig. 6(c). For compensating the phase error at downlink frequency as shown in Fig. 6(b), a lower delay line of increasing length on the outermost ring controlled by PIN diode, D3 is implemented. The optimized length of the delay line, as shown in Fig. 6(a), offers a phase range of 415° at 12.2 GHz. Similarly, for the X band, the phase error needs to be compensated as shown in Fig. 7(c). Finally, Fig. 8 depicts the length of the delay line required for phase compensation by switching ON diodes D3 and D4 at downlink and X-band frequencies.

Based on the simulated results of the unit cell, a frequency reconfigurable reflectarray consisting of 15×15 elements is designed with a periodicity of 10.5 mm $(0.49\lambda_0)$ as shown in Fig. 9. The 225 elements of the RA are set on a square plane geometry of $167.5mm \times 167.5mm$ in size. A MATLAB program calculates the required continuous phases for unit cell central locations in the

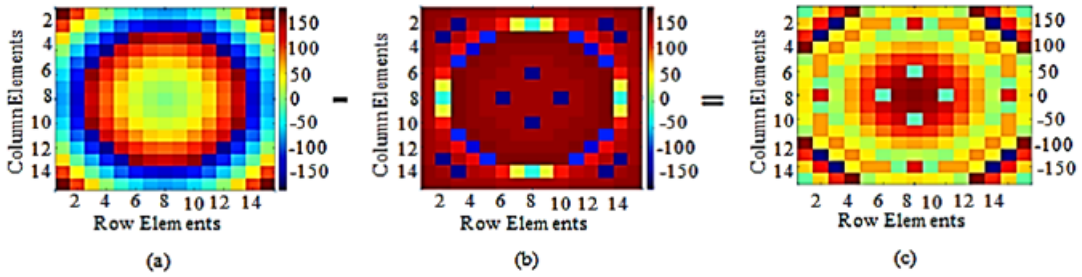

Figure 6. Calculation for Downlink Design (a) Phase Difference at each unit cell, (b) Phase Shift at 12.2 GHz, (c) Phase Error at 12.2 GHz

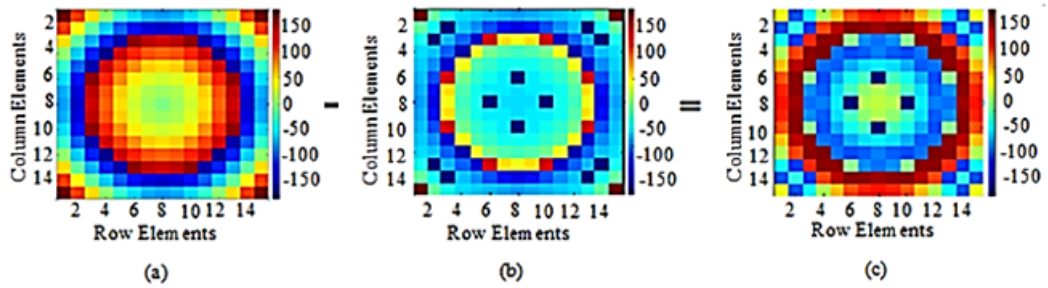

Figure 7. Calculation for X band Design (a) Phase Difference at each unit cell, (b) Phase Shift at 11.9 GHz, (c) Phase Error at 11.9 GHz

RA, using which the user selects the range of phase values that should correspond to a certain discrete phase.

The unit cell parameters required to generate that particular discrete phase are fed to an EM simulator instance in the CST project in MATLAB for building a unit cell. This procedure is repeated for each location of the unit cell in the RA.

Similarly, the phase error for the X-band design is estimated, as depicted in Fig. 6(c), from the difference between the simulated phase response of the downlink unit cell and the phase shift required for X-band operation. Based on this phase error result as shown in Fig. 7(c), the length of the delay line is optimized as given in Fig. 7(b), and the fourth PIN diode D4 is integrated into the upper delay line. This diode is switched ON to obtain a phase shift of 308° at an X-band frequency of 11.9 GHz.

The length of the delay lines in every unit cell of the array is varied by switching ON and OFF the D3 and D4 PIN diodes at 12.2 GHz and 11.9 GHz as shown in Fig. 6(a) and 7(a) respectively. Table 2 summarizes the operations of these PIN diodes for uplink and downlink frequency bands. In the frequency band around 11.9 GHz, especially the reactance of the diode needs to be considered carefully.

In the OFF state, the length of the delay line does not get affected. While in the ON state, the capacitance of the diode adds an effective length to the delay line. When switched ON, the physical length of the diode and its inductance also add a specific phase to the reflection phase of the element. The diode can be seen as a delay line that adds a phase offset to the phase of the re-radiated field.

In the proposed design, 900 PIN diodes are used to switch between the two states of the phase as a suitable measure to accomplish electronic reconfiguration. The PIN diode MACOM MADP-000907-14020 manufactured by MACOM matches the demands of an operating frequency of Ku-band and X-band. However, at such a high frequency, the loss and phase shift induced by the diode has to be considered carefully.

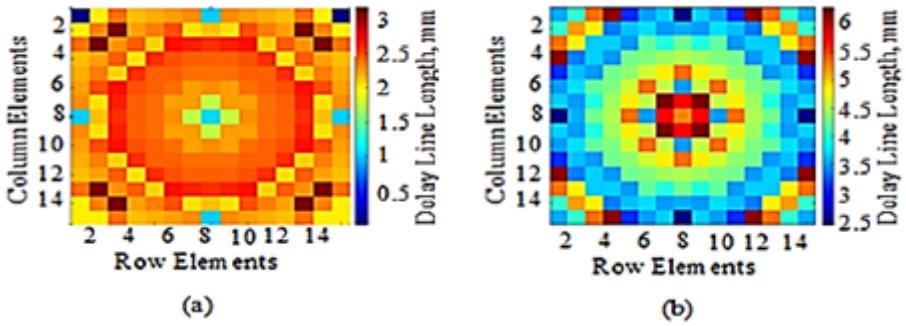

Figure 8. Optimized Delay line length (a) At 12.2 GHz (b) 11.91 GHz

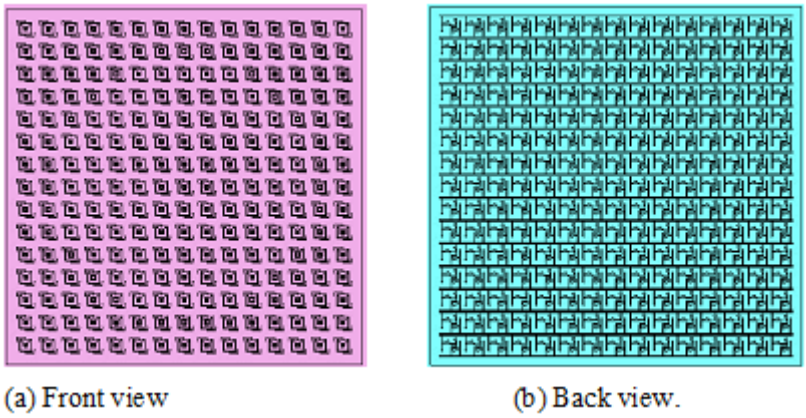

Figure 9. A 15×15 RRA prototype

Driving the PIN diode with a low current reduces the power consumption of the RA considerably. As the diode is not an ideal switch but has a finite resistance in the off state and a small resistance in the ON state, its behaviour has to be included in the design process of the element.

The designed RRA is simulated using a Ku−band standard pyramidal horn having a flare length of 54 mm connected to a waveguide of $20mm \times 15mm$ aperture size. It is designed for a gain of 14 dB at 15 GHz. The pyramidal horn antenna is placed at a focal distance (F) of 134 mm from the center of the RA. Considering 0.8 as the F/D ratio, the measured E and H plane feed taper values are found to be 8 dB and 8.7 dB, respectively, and the H plane value is 6.5 dB.

The aperture efficiency is calculated based on the following Eq. 4:
Aperture efficiency,

$$(\eta) = G\frac{\lambda^2}{4\pi A} \tag{4}$$

4. Results and Discussions

This section presents and discusses the RA prototype along with the simulated results of the proposed RRA. The simulated results are obtained with the time domain solver of the CST Microwave Studio. The gain and far-field radiation patterns are obtained to validate the performance of the designed RRA. Figure 10 represents the E-plane and H-plane simulated radiation patterns of the proposed RRA at the uplink, downlink, and X-band frequencies. The E- and H-plane simulated radiation patterns depicts a 3 dB beamwidth of 7.3 °, 8.6 °, and 9.0 ° at the operating frequencies of 14.34 GHz, 12.2 GHz, and 11.9 GHz, respectively. The simulated sidelobe levels are -17.1 dB, -13.6 dB, and -16.3 dB at 14.34 GHz, 12.2 GHz, and 11.9 GHz, respectively. The cross-polarization levels are -17.14 dB, -10.15 dB, and -22.79 dB below the maximum values at 14.4 GHz, 12.2 GHz, and 11.9 GHz, respectively. The maximum simulated gain of the RRA at 14.34 GHz is 25.55

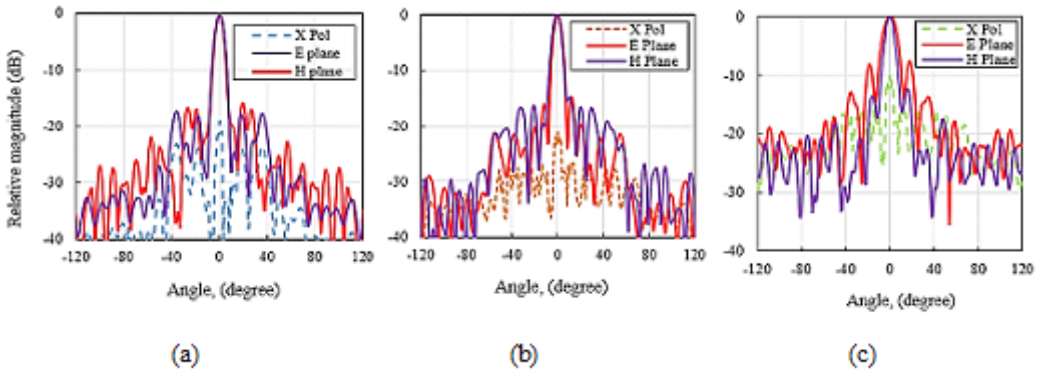

Figure 10. Simulated E, H-plane patterns and cross-polarizations at (a) 14.34 GHz, (b) 12.2 GHz, and (c) 11.9 GHz

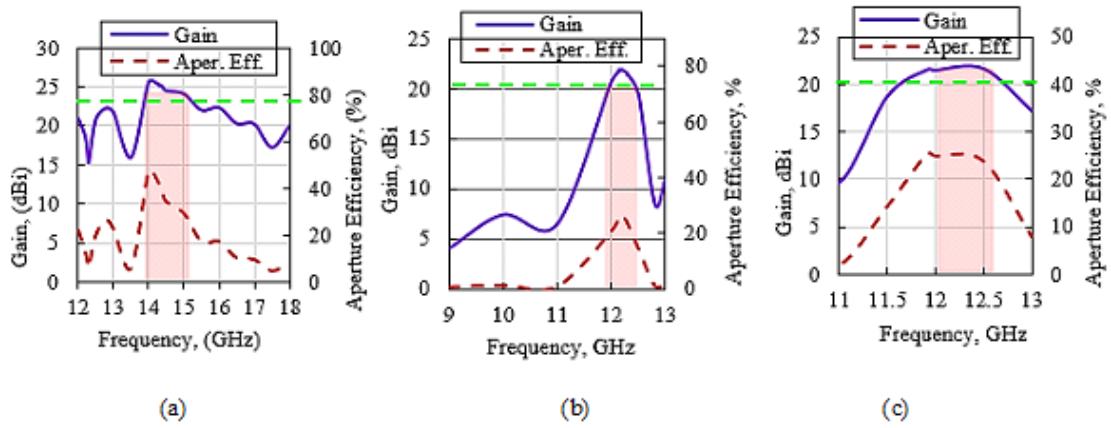

Figure 11. Simulated gain and aperture efficiency vs frequency plot at (a) 14.34 GHz, (b) 12.2 GHz, and (c) 11.9 GHz

dB. At the downlink frequency of 12.2 GHz and the X-band frequency of 11.9 GHz, the simulated gains of 24.86 dB and 22.65 dB are obtained, respectively. At the operating frequency of 14.34 GHz, 8.37% of a -3 dB gain bandwidth is obtained. Similarly, 4.92% and 12.18% bandwidths are achieved at 12.2 GHz and 11.9 GHz, respectively. The aperture efficiency is calculated at the three operating frequencies as 40.22%, 26.46%, and 25.36%, respectively. The variation of gain and aperture efficiency across the frequency bands of uplink, downlink, and X-band operation is shown in Fig. 11.

The reduced aperture efficiency at downlink and X-band frequencies may be due to the inadequate edge illumination feed taper of 6.5 dB and rectangular symmetric feed horn illumination. Other factors that cause a reduction in aperture efficiency are blockage effects and multiple scattering between the feed horn and the RRA structure.

Table 4 explains the performance of the proposed RA in comparison with previous works explained in the literature survey. The following inferences are derived from the comparison in Table 4 that are as follows:

1. The proposed unit element offers increased phase variations of 525 °, 415 °, and 308 ° over a frequency range of 14.34 GHz, 12.2 GHz, and 11.9 GHz, which is higher compared to those in (Tayebi et al., 2015), (Yang et al., 2017), & (Han et al., 2004).

2. The proposed RA offers a better 1 dB gain bandwidth of 8.37%, 4.92%, and 12.18% at respective frequencies than the RA reported in (Tayebi et al., 2015), (Yang et al., 2017), &

(Han et al., 2004).

3. The number of elements is 225, which is less compared to those in (Malfajani and Atlasbaf, 2014), (Tayebi et al., 2015) & (Yang et al., 2017).

4. The simulated aperture efficiency (%) of 40.22, 26.4, and 25.36 for the uplink, downlink, and X-band frequencies are higher compared to that reported in (Malfajani and Atlasbaf, 2014), (Tayebi et al., 2015) & (Yang et al., 2017).

Table 4. Comparison With Previous Works

	Current work	**(Yang et al., 2017)**	**(Tayebi et al., 2015)**	**(Malfajani and Atlasbaf, 2014)**	**(Han et al., 2004)**
Center frequency (GHz)	14.34/12.2/11.9	11.1/14.3	5.30/3.49	22/10	7.3/31.75
Attainable phase range (Degrees)	525/415/308	180 ±22.5	335/340	800/500	360/360
Aperture size (λ)	15.92	40	10	8.5	15.3%
Simulated Gain (dBi)	25.5/24.86/22.65	29.3/30.8	–	29.7/26.2	28.2/40.3
Simulated aperture efficiency (%)	40.2/26.46/25.36	21.6/18.1	–	25/47	46/38
-1 dB Gain Bandwidth	8.37/4.92/12.18%	0.35 GHz/0.7 GHz	–	9.1/16%	7.1/6.3
SLL (dB)	-17.1/-13.6/-16.3	<-18	-	<-16	<-17.5
No. of Elements	225	1600	100	828	437,9236
Active elements	PIN	PIN	Varactor	None	None

5. Conclusion and Future scope

In this paper, a novel dual−band, single−layer, frequency RRA with 15 × 15 elements of $167.5mm \times 167.5mm$ in size is presented. The unit cell comprises three concentric square loops, with two inner loops being varied for achieving 525° at the uplink frequency with PIN diodes in OFF state condition. For downlink and X-band frequencies, with the PIN diode in ON state condition, phase compensation of 415° and 308° is achieved by varying delay lines attached to the outer square loop. The unit cell was simulated using CST simulation software with plane wave excitation. A Ku-band standard-gain pyramidal horn antenna is used for measurement purposes. The maximum simulated gain of the RRA at 14.34 GHz is 25.55 dB. At the downlink frequency of 12.2 GHz and the X-band frequency of 11.9 GHz, the simulated gains of 24.86 dB and 22.65 dB are obtained, respectively. At the operating frequency of 14.34 GHz, 8.37% of the -3 dB gain bandwidth is shown. Similarly, 4.92% and 12.18% bandwidths are calculated at 12.2 GHz and 11.9 GHz, respectively. The aperture efficiency is calculated at the three frequencies as 40.22%, 26.46%, and 25.36%, respectively. Compared to previous works analysed in the literature survey, this paper achieves a gain of more than 20 dBi in all three frequency ranges. In this paper, the X-band far-field radiation pattern is not obtained within the mid-band frequency range. This can be resolved by implementing further improvements in an array structure.

References

Abdelrahman, A. H; Liang, M, and Xin, H. Reconfigurable reflectarray antenna for microwave detection and imaging. volume 2017-January, 2017. doi: 10.1109/APUSNCURSINRSM.2017.8073076.

Arslan, M and Alamgir, S. Performance optimization of unit-cell reflectarray antenna for future 5g communications. *International Journal of Computer Applications*, 174, 2017. doi: 10.5120/ijca2017915343.

Barriuso, I; Gutierrez, A. L; Lanza, M; Domingo, M; Perez, J. R; Valle, L, and Basterrechea, J. Analysis of single layer multiple concentric ring elements in reflectarray antennas. 2011. doi: 10.1109/APS.2011.5996435.

Bayraktar, O; Civi, O. A, and Akin, T. Beam switching reflectarray monolithically integrated with rf mems switches. *IEEE Transactions on Antennas and Propagation*, 60, 2012. ISSN 0018926X. doi: 10.1109/TAP.2011.2173099.

Carrasco, E; Barba, M, and Encinar, J. A. X-band reflectarray antenna with switching-beam using pin diodes and gathered elements. *IEEE Transactions on Antennas and Propagation*, 60, 2012. ISSN 0018926X. doi: 10.1109/TAP.2012.2208612.

Chen, Y; Chen, L; Wang, H; Gu, X. T, and Shi, X. W. Dual-band crossed-dipole reflectarray with dual-band frequency selective surface. *IEEE Antennas and Wireless Propagation Letters*, 12, 2013. ISSN 15361225. doi: 10.1109/LAWP.2013.2280891.

Encinar, J. A and Zornoza, J. A. Three-layer printed reflectarrays for contoured beam space applications. *IEEE Transactions on Antennas and Propagation*, 52, 2004. ISSN 0018926X. doi: 10.1109/TAP.2004.827506.

Fusco, V. F. Mechanical beam scanning reflectarray. *IEEE Transactions on Antennas and Propagation*, 53, 2005. ISSN 0018926X. doi: 10.1109/TAP.2005.858828.

Guclu, C; Perruisseau-Carrier, J, and Civi, O. A. Proof of concept of a dual-band circularly-polarized rf mems beam-switching reflectarray. *IEEE Transactions on Antennas and Propagation*, 60, 2012. ISSN 0018926X. doi: 10.1109/TAP.2012.2207690.

Han, C; Rodenbeck, C; Huang, J, and Chang, K. A c/ka dual frequency dual layer circularly polarized reflectarray antenna with microstrip ring elements. *IEEE Transactions on Antennas and Propagation*, 52, 2004. ISSN 0018926X. doi: 10.1109/TAP.2004.835144.

Han, J; Li, L; Liu, G; Wu, Z, and Shi, Y. A wideband 1 bit 12×12 reconfigurable beam-scanning reflectarray: Design, fabrication, and measurement. *IEEE Antennas and Wireless Propagation Letters*, 18, 2019. ISSN 15485757. doi: 10.1109/LAWP.2019.2914399.

Hu, W; Cahill, R; Encinar, J. A; Dickie, R; Gamble, H; Fusco, V, and Grant, N. Design and measurement of reconfigurable millimeter wave reflectarray cells with nematic liquid crystal. *IEEE Transactions on Antennas and Propagation*, 56, 2008. ISSN 0018926X. doi: 10.1109/TAP.2008.929460.

Hum, S. V; Okoniewski, M, and Davies, R. J. Realizing an electronically tunable reflectarray using varactor diode-tuned elements. *IEEE Microwave and Wireless Components Letters*, 15, 2005. ISSN 15311309. doi: 10.1109/LMWC.2005.850561.

Kamoda, H; Iwasaki, T; Tsumochi, J; Kuki, T, and Hashimoto, O. 60-ghz electronically reconfigurable large reflectarray using single-bit phase shifters. *IEEE Transactions on Antennas and Propagation*, 59, 2011. ISSN 0018926X. doi: 10.1109/TAP.2011.2152338.

Li, Y and Abbosh, A. Reconfigurable reflectarray antenna using single-layer radiator controlled by pin diodes. *IET Microwaves, Antennas and Propagation*, 9, 2015. ISSN 17518733. doi: 10.1049/iet-map.2014.0227.

Liu, G; Wang, H; Xue, F; Zhu, D, and Dong, X. A wideband reconfigurable reflectarray antenna using single-layer varactor-loaded split patch elements. volume 2018, 2018. doi: 10.1049/cp.2018.1127.

Luyen, H; Zhang, Z; Booske, J. H, and Behdad, N. Wideband, beam-steerable reflectarrays based on minimum-switch topology, polarization-rotating unit cells. *IEEE Access*, 7, 2019. ISSN 21693536. doi: 10.1109/ACCESS.2019.2904249.

Malfajani, R. S and Atlasbaf, Z. Design and implementation of a dual-band single layer reflectarray in x and k bands. *IEEE Transactions on Antennas and Propagation*, 62, 2014. ISSN 0018926X. doi: 10.1109/TAP.2014.2327137.

Murugesan, A; Natarajan, D, and Selvan, K. T. Low-cost, wideband checkerboard metasurfaces for monostatic rcs reduction. *IEEE Antennas and Wireless Propagation Letters*, 20, 2021. ISSN 15485757. doi: 10.1109/LAWP.2021.3054863.

Perez-Palomino, G; Baine, P; Dickie, R; Bain, M; Encinar, J. A; Cahill, R; Barba, M, and Toso, G. Design and experimental validation of liquid crystal-based reconfigurable reflectarray elements with improved bandwidth in f-band. *IEEE Transactions on Antennas and Propagation*, 61, 2013. ISSN 0018926X. doi: 10.1109/TAP.2013.2242833.

Perez-Palomino, G; Barba, M; Encinar, J. A; Cahill, R; Dickie, R; Baine, P, and Bain, M. Design and demonstration of an electronically scanned reflectarray antenna at 100 ghz using multiresonant cells based on liquid crystals. *IEEE Transactions on Antennas and Propagation*, 63, 2015. ISSN 0018926X. doi: 10.1109/TAP.2015.2434421.

Perruisseau-Carrier, J and Skrivervik, A. K. Monolithic mems-based reflectarray cell digitally reconfigurable over a 360° phase range. *IEEE Antennas and Wireless Propagation Letters*, 7, 2008. ISSN 15361225. doi: 10.1109/LAWP.2008.919327.

Pozar, D. M. Bandwidth of reflectarrays. *Electronics Letters*, 39, 2003. ISSN 00135194. doi: 10.1049/el:20030990.

Tayebi, A; Tang, J; Paladhi, P. R; Udpa, L; Udpa, S. S, and Rothwell, E. J. Dynamic beam shaping using a dual-band electronically tunable reflectarray antenna. *IEEE Transactions on Antennas and Propagation*, 63, 2015. ISSN 0018926X. doi: 10.1109/TAP.2015.2456939.

Venneri, F; Costanzo, S; Massa, G. D; Borgia, A; Corsonello, P, and Salzano, M. Design of a reconfigurable reflectarray based on a varactor tuned element. 2012. doi: 10.1109/EuCAP.2012.6206624.

Venneri, F; Costanzo, S, and Massa, G. D. Design and validation of a reconfigurable single varactor-tuned reflectarray. *IEEE Transactions on Antennas and Propagation*, 61, 2013. ISSN 0018926X. doi: 10.1109/TAP.2012.2226229.

Wu, B; Sutinjo, A; Potter, M. E, and Okoniewski, M. On the selection of the number of bits to control a dynamic digital mems reflectarray. *IEEE Antennas and Wireless Propagation Letters*, 7, 2008. ISSN 15361225. doi: 10.1109/LAWP.2008.920908.

Yang, H; Yang, F; Cao, X; Xu, S; Gao, J; Chen, X; Li, M, and Li, T. A 1600-element dual-frequency electronically reconfigurable reflectarray at x/ku-band. *IEEE Transactions on Antennas and Propagation*, 65, 2017. ISSN 0018926X. doi: 10.1109/TAP.2017.2694703.